

Quantum dynamics in phase space: From coherent states to the Gaussian representation

P. D. Drummond⁽¹⁾, P. Deuar^{(2)†}, T. G. Vaughan⁽¹⁾ and J. F. Corney⁽¹⁾

⁽¹⁾ARC Centre of Excellence for Quantum-Atom Optics,
School of Physical Sciences, University of Queensland,
Brisbane, QLD 4072, Australia

⁽²⁾Van der Waals-Zeeman Instituut, Universiteit van Amsterdam,
1018 XE Amsterdam, Netherlands

[†]Present address: LPTMS, Bât. 100, Université Paris-Sud 91405 Orsay cedex, France

February 2, 2008

Abstract

We give an outlook on the future of coherence theory and many-body quantum dynamics as experiments develop in the arena of ultra-cold atoms. Novel results on quantum heating of center-of-mass temperature in evaporative cooling and simulation methods for long-range interactions are obtained, using positive-P phase-space techniques.

1 Coherence theory in the 21st century

One recognition of important developments in coherence theory was the 2005 Nobel award in Physics, one half to Roy J. Glauber, ‘*for his contribution to the quantum theory of optical coherence*’, and one half to Ted Haensch and Jan Hall ‘*for their contributions to the development of laser-based precision spectroscopy*’. This richly deserved award recognizes crucial developments in quantum optics and laser science in the second half of the twentieth century. One may ask now: ***What is the future of coherence theory?***

One answer to this question lies in the groundbreaking work of experimentalists working with ultra-cold atoms. Perhaps the ideal quantum system for experimental investigation, ultracold atoms display many useful properties under active investigation, including:

- Ultra-low temperatures to below 1nK
- Bose-Einstein condensates (BEC): atom ‘photons’
- Quantum superfluid degenerate Fermi gases (DFG): atom ‘electrons’

- ‘Superchemistry’: stimulated bosonic molecule formation
- Atom lasers, atomic diffraction, atom interferometers
- Direct detection of atom coherence and correlations

A crucial, common property of photons and ultracold gases is their *simplicity* as many-body systems. This makes them ideal candidates for both theoretical and experimental investigation in fundamental science. The underlying interactions are well understood, the experimental systems can be easily characterized by a few parameters, and interaction strengths can be tuned.

Under these conditions, well-known theoretical models can be used to high accuracy, thus combining ideas from coherence and many-body theory. As well as being able to test and understand theories like the Hubbard model, one has the possibility of new technologies of unprecedented accuracy and subtlety. This is likely to lead to new tests of macroscopic quantum mechanics and quantum superpositions, which is undoubtedly one of the grand challenges of modern physics.

In this paper, we give a brief overview of recent directions that coherence theory has taken since it originated in the quantum optics area, as well as giving new theoretical results on examples of quantum dynamics. First we describe some of the recent experimental developments in quantum-atom optics, in which the role of correlations are becoming increasingly important. Second, we review theoretical developments in which coherence theory is being utilized to give new simulation techniques that can handle the fundamental issue of quantum dynamics of many-body systems.

2 Quantum dynamical experiments

As one of the new types of experiment on atomic coherence and correlations, many laboratories are now able to carry out intrinsically *dynamical* experiments on many-body systems, rather than the near-equilibrium experiments of condensed matter physics. Dynamical results provide a new probe into the properties of many-body systems. Clearly, the future of coherence theory must include an understanding of how to quantitatively predict the results of experiments involving the dynamical evolution of many-body quantum systems far from thermal equilibrium. Due to the rapid growth of ultra-cold atom facilities, these types of experiment are now carried out in many laboratories. They test quantum theory in regimes of large particle number, as they typically involve $10^2 - 10^7$ interacting particles, at temperatures of around 100nK.

A schematic diagram of the type of experiment that we will focus on is shown in Fig (1). A condensate is prepared with each atom in a quantum superposition of two different momenta, resulting in effectively two condensates in relative motion, occupying the same physical space. Subsequently, a strong scattering commences, in which both individual particle and coherent many-body effects play important roles.

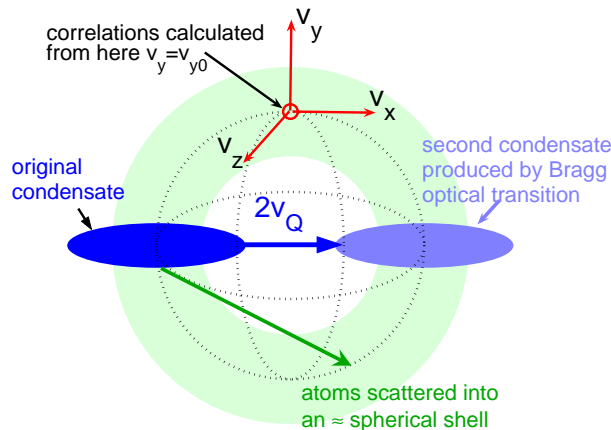


Figure 1: Momentum-Space Diagram of an ultra-cold collision experiment.

In the remainder of this section, we will outline two recent experiments of this type, in which many-body effects clearly play a role. There are other experiments as well, and indeed this is a very rapidly developing field.

2.1 Collisions in Sodium BEC

An example of quantum dynamics is provided by a series of experiments by the Ketterle group at MIT[1] that involve the three-dimensional collision of two sodium (Na) BECs, as in the schematic diagram of Fig (1). The two BECs are produced from a single initially ellipsoidal trapped cloud, as found in a non-spherical magnetic trap.

The initial condensate is then split into two halves, with a large relative velocity, and the trap is turned off. This leaves two condensates that are spatially overlapped and have a relative velocity, so that a collision occurs. Also observed in these experiments are: amplification of seed pulses during a collision, interaction of condensates with lattices, and quantum reflection from a mirror. These condensates typically include 10^7 or more interacting bosons, and measurements usually involve the observation of density distributions.

2.2 Metastable Helium experiments

A recent experimental configuration that allows the retrieval of much more information is the interaction of metastable Helium condensates. These have a distinct advantage over the alkali metals like sodium or rubidium, in that single atom arrivals at a detector multi-channel plate can be readily detected, owing to the high excitation energy (around 20eV) of the metastable atoms. This allows atomic correlations to be measured directly[2].

Metastable helium experiments have been carried out by a number of groups. In particular, the group of Westbrook and Aspect at the Institut d'Optique

(France) have already observed three-dimensional collisions of metastable He^* , using multichannel plate (MCP) detection combined with a time-domain multiplexor to obtain both temporally and spatially resolved quantum correlations of atomic arrival times[3, 4]. Backward and forward quantum correlations were observed to be enhanced. A similar experiment is also underway by Truscott[5] at The Australian National University.

3 Many-body quantum dynamics

The well-known difficulty with treating the dynamical quantum theory of many-body systems, is that the Hilbert space — the number of quantum states involved — can become exponentially complex. This is a subtle point, as of course given an exact solution, a system in a pure state is described by just one quantum state at all times. The problem is that when one does not know the relevant exact quantum state, it is necessary to expand in a basis of states.

3.1 Exponential complexity

As an example, consider n atoms distributed among m modes, with $n \simeq m \simeq 500,000$. The number of possible many-body number states that could be involved is:

$$N_s = 2^{2n} = 2^{1,000,000} \quad (1)$$

Since this number means that there are more quantum states than atoms in the universe, we conclude that even on the largest possible computer, we can't diagonalize the Hamiltonian relative to this basis, in general!

3.2 Traditional theoretical methods

There are many traditional theoretical methods, which all have severe drawbacks as first principles solutions:

1. Perturbation theory. A well established approach, perturbation theory can be applied in many ways, and a particularly sophisticated variation is obtained by using perturbation theory on a path-integral formulation of quantum dynamics. This approach diverges at strong couplings and long times.
2. Operator factorization. This approach neglects any quantum correlations. Although many variations exist, these methods inherently involve uncontrolled approximations, and are not applicable for strong correlations.
3. Restricted Hilbert-spaces. Complementary to the idea of operator factorization is the approximation of using a truncated Hilbert space, with an unknown error due to the truncation. Examples in this general category include the density matrix renormalization method[6]. Similarly, density functional theory[7] has unknown approximation errors.

4. Numerical diagonalisation. While exact in principle, this is intractable for large particle numbers, unless the number of spatial modes is severely restricted.
5. Bethe ansatz solutions. Certain one-dimensional many-body problems have exactly known eigenstates from the Bethe ansatz. These can be very useful in static cases. However, knowing the eigenvalues does not necessarily solve the dynamical complexity problem. Exponentially many eigenstates are still required to expand an arbitrary initial state — there are simply too many basis states for exact quantum dynamical calculations.
6. Quantum computers. Can quantum computers solve quantum dynamics? In 1982, Feynman proposed this approach. By even the most optimistic predictions, hardware of practical use is still many years away, and their range of application appears limited.

In summary, we see that while experimentalists have more sophisticated tools than ever before, the theorist faces severe difficulties in modeling these new experiments. It would clearly be useful to have first-principles techniques that utilize existing computers.

3.3 Classical phase space

One of the most important and enduring ideas of Glauber[8], developed in parallel with an approach of Sudarshan[9], was the use of coherent states to generate quantum operator representations for bosons. In some cases one can obtain expansions of the density matrix using a probability $P(\vec{\alpha})$. For an M -mode bosonic problem, we define:

$$\hat{\rho} = \int P(\vec{\alpha}) |\vec{\alpha}\rangle \langle \vec{\alpha}| d^{2M} \vec{\alpha} . \quad (2)$$

where $|\vec{\alpha}\rangle$ is an M -mode coherent state, defined as a simultaneous eigenstate of the annihilation operators. This approach maps quantum states into an essentially classical phase-space. We note that there is a clear limitation here: the expansion is a separable one, and therefore cannot describe entangled states.

The technique, of course, was highly successful in its applications to the quantum theory of the laser, since a laser output state is typically non-entangled. Different variations of this approach are obtained by considering different operator orderings in the equivalence relations between operator products and classical field products. Many prominent physicists have developed and used phase-space distributions for quantum systems, starting from Wigner[10] and Husimi[11], with later developments due to Glauber, Sudarshan, Agarwal and Wolf[12, 13], Lax[14] and many others.

The problem, however, with interpreting these distributions as probabilistic mappings to a classical phase space is that these are fundamentally incomplete. When used to calculate general quantum dynamical time-evolution, either the distributions or the propagators can have negative values. Even the Husimi

Q-function, which is statically complete and always positive, generally has no corresponding positive propagator. Hence, no stochastic process is available for simulation purposes.

3.4 Quantum phase space

The problems of exponential complexity can be reduced — though not wholly eliminated — by using a doubled phase-space expansion that allows quantum superpositions and entanglement in the basis set. The idea of dimension-doubling was also proposed by Glauber[8]. However, this by itself is not sufficient. It is also necessary to have an appropriate differential mapping, which maps the operator products that occur in a physical Hamiltonian, to positive definite differential operators that have stochastic equivalences.

The first approach of this type was the positive-P representation[15, 16], in which there are $2M$ complex coordinates, so that:

$$\hat{\rho} = \int P(\vec{\alpha}, \vec{\beta}) \frac{|\vec{\beta}\rangle\langle\vec{\alpha}|}{\langle\vec{\alpha}|\vec{\beta}\rangle} d^{2M}\vec{\alpha} d^{2M}\vec{\beta} \quad (3)$$

The resulting distributions are positive and obey a diffusion equation, so that they can be effectively simulated using a stochastic process.

3.5 Application

Before turning to specific examples, we give the $+P$ equations for a general bosonic system with two-body interactions. Such systems are modeled by using nonlinear interactions on a lattice, together with linear interactions coupling different sites, so that the quantum Hamiltonian is:

$$\hat{H}(\mathbf{a}, \mathbf{a}^\dagger) = \hbar \sum_{ij} \left[\omega_{ij} a_i^\dagger a_j + \frac{1}{2} \chi_{ij} : \hat{n}_i \hat{n}_j : \right]. \quad (4)$$

Here ω_{ij} is a nonlocal linear coupling, which may correspond to simple quantum diffusion of free particles, or else to inter-well hopping in the case of a true lattice, while χ_{ij} is a nonlocal nonlinear coupling. If $\chi_{ij} = \chi \delta_{ij}$, then one recovers the usual local interaction lattice theory, applicable for ultracold atoms under s-wave scattering. The boson number operator at each site is: $\hat{n}_i = a_i^\dagger a_i$, which has a stochastic equivalent of $n_i = \beta_i^* \alpha_i$. Even though the Hamiltonian has the appearance of modeling a lattice, the general approach also holds for quantum fields with a momentum cut-off that equals the inverse lattice spacing.

With the addition of nonlocal linear damping of κ_{ij} , the simplest corresponding positive-P stochastic equations have the Itô form:

$$\frac{\partial \alpha_i}{\partial t} = -(\kappa_{ij} + i\omega_{ij}) \alpha_j - \left(i\chi_{ij} n_j + b_{ik} \eta_k^{(a)}(t) \right) \alpha_i$$

$$\frac{\partial \beta_i}{\partial t} = -(\kappa_{ij} + i\omega_{ij})\beta_j - \left(i\chi_{ij}n_j^* + b_{ik}\eta_k^{(b)}(t)\right)\beta_i \quad (5)$$

Here the noise matrix \mathbf{b} is the solution to $b_{ik}b_{jk} = -i\chi_{ij}$, and the noises are delta correlated, so that $\langle \eta_i^{(a)}(t)\eta_j^{(a')}(t') \rangle = \delta_{ij}\delta^{(a,a')}\delta(t-t')$.

The earliest example of this technique was the prediction of quantum squeezing of solitons in optical fibres[17], using the positive-P representation. In this case the relatively high occupations of modes means that a truncated form of the Wigner representation is also very useful. These predictions have been recently confirmed to high accuracy. There are many other applications, including simulation of evaporative cooling[18], spin squeezing [19], correlation dynamics in a uniform gas[20], the quantum evolution of large numbers number of interacting atoms in a single well[21], the dynamics of atoms in a 1D trap[22], and molecular down-conversion to atoms[23].

4 Examples

In the remainder of this paper, we shall focus on some novel results.

4.1 Direct quantum simulations of BEC formation

A thorough treatment of the initial state of a quantum experiment ideally should include a theory of state-preparation. While it is certainly possible to use phase-space techniques starting from the common assumption of a canonical ensemble at finite temperature, there is a more fundamental question of interest in ultra-cold atom Bose-Einstein condensation. Is the concept of a thermal equilibrium at finite temperature always applicable in these experiments? This question arises because the experiments are fundamentally non-equilibrium in nature, with no external reservoir at a fixed temperature as in most condensed matter experiments.

The true state of an atom laser or BEC is the result of cooling through evaporation. Therefore to try to answer this question, one must simulate the actual evaporative cooling process that leads to condensate formation. The process itself is depicted schematically in Fig (2). Collisions of hot atoms lead to condensate formation together with the escape of even hotter atoms from the trap, as there is an overall energy conservation in the collisions.

In our simulations, we use a model identical to that used in[18]: a small $(3+1)$ D system with an initial 240nK thermal distribution. We suppose there are $N = 10^4$ bosonic atoms of mass $m = 1.5 \times 10^{-25}$ kg, initially confined to a box of side $L = 10\mu\text{m}$. At $t = 0^+$ a smooth trapping potential is switched on. It is of the form

$$V(\vec{x}, t) = V_0(1 - t/t_0) \sum_{j=1}^D \sin^2\left(\frac{\pi x_j}{2L}\right) \quad (6)$$

where $k_B V_0$ is similar to the initial temperature and t_0 is the length of the relaxation — about 100ms. This potential is chosen so that atoms can escape

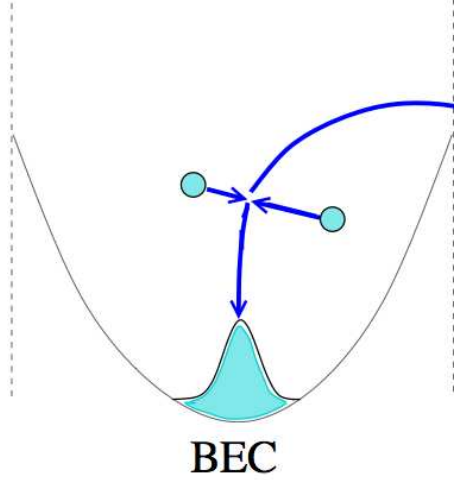


Figure 2: diagram of the physics of evaporative cooling. Two atoms collide, one losing energy and becoming condensed, while the other gains energy and escapes from the trap.

more readily as time evolves, which should lead to a continual lowering in the average energy of the remaining atoms. This cooling strategy also reduces the effective trap frequency with time, leaving a cloud of untrapped atoms at the end of the process. In the simulations, the lattice boundary is absorbing, so that atoms reaching the edge of the simulation region are simply removed through localized linear damping.

4.1.1 Definition of COM temperature

While it is widely accepted that the evaporative cooling strategy leads to formation of a Bose-Einstein condensate, the question of which mode is condensed is not so easily answered. Simulations indicate that the condensate is in motion, with a center of mass effective temperature that may both increase as well as decrease during evaporative cooling. In other words, while the relative motion of particles is being cooled, it is possible for the center-of-mass to become hotter, since these degrees of freedom are largely decoupled.

We can directly apply the equipartition theorem to arrive at an estimate of the COM temperature. We assume that the COM energy can be written

$$E_{COM} \sim \frac{\langle |\vec{P}|^2 \rangle}{2m\langle \hat{N} \rangle} + \frac{1}{2}m(\omega_{\text{eff}}(t))^2 \frac{\langle |\hat{N}\vec{X}|^2 \rangle}{\langle \hat{N} \rangle} \quad (7)$$

where $\omega_{\text{eff}}(t)$ is obtained from $V(\vec{x}, t)$ by assuming small deviations of the COM position from zero, in which case $\sin^2 x \simeq x^2$. We then estimate that the effective

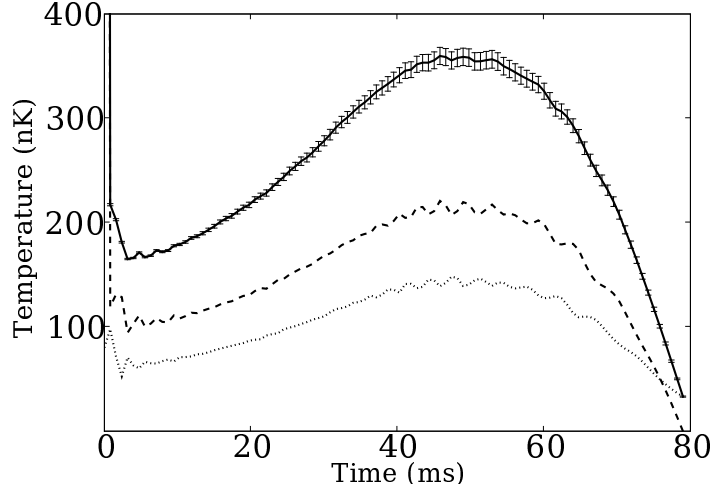


Figure 3: Full 3D positive-P results for COM heating. The solid curve represents the full COM temperature estimate, where the large initial spike is due to the rapid switch-on of the trap. The dotted and dashed curves represent the contributions of kinetic and potential energy respectively.

temperature is given by

$$T_{COM} \simeq \frac{E_{COM}}{Dk_B} \quad (8)$$

where D represents twice the number of COM degrees of freedom (eg. 6 for a trapped 3D gas).

4.1.2 Positive-P simulation results

Fig (3) gives a full three-dimensional simulation of this evaporative cooling scenario, focusing on the effective temperature of the center-of-mass.

It is clear from these results that a strong evaporative heating of the center-of-mass degree of freedom occurs simultaneously with the evaporative formation of a Bose condensate. This can be understood from physical arguments. The Bose enhancement of scattering into moving modes randomly condenses the gas into a moving condensate. Here the coherence properties of the gas means that all the condensed atoms have the same velocity, which enhances the effective center-of-mass temperature, even while the condensate forms. The final cooling of the center-of-mass temperature is due to enhanced evaporative losses of more rapidly moving condensates, as the trap walls are lowered. We note here that these results are limited by the sampling error, depicted by the error bars in the figure.

4.2 Long-range or strong particle interactions

The positive-P and related phase-space representations are also readily applicable to strongly interacting situations where the range or shape of the interparticle interaction cannot be ignored. Quantitative dynamics for such systems have been very difficult to obtain apart from some special systems.

Here, instead of pre-calculating scattering behaviour for two- (or more-) body collisions, we remain with the raw Hamiltonian that explicitly gives an interparticle potential. This corresponds to the nonlocal form of the lattice Hamiltonian given above. As a proof of principle, we have calculated the dynamics of a small strongly interacting cloud of cold bosons confined in a one-dimensional trap whose width is of the same size as the range of the interparticle potential[24].

At $t < 0$, bosons with negligible interparticle interaction are prepared in a harmonic trap with trapping potential $V^{\text{ext}}(x) = \frac{1}{2} m \omega_{\text{ho}}^2 x^2$, which has a harmonic oscillator length $a_{\text{ho}} = \sqrt{\hbar/m\omega_{\text{ho}}}$. Initially they are in the coherent zero-temperature ground state obtained by solving the Gross-Pitaevskii mean field equations[25]. The mean number of atoms in the trap in this example is $\bar{N} = 10$ ($\bar{N} = 100$ was also simulated, albeit for a shorter time span). At $t = 0$, interparticle interactions are turned on across the system. This kind of effect is most commonly induced in practice by utilizing a Feshbach resonance. A “breathing” of the atomic cloud is also induced by switching the trap to a more confined harmonic potential with double the trapping frequency.

We model the interparticle interactions by a Gaussian interparticle potential

$$U(x) = \gamma (\hbar \omega_{\text{ho}}) \left(\frac{1}{\sigma_U \sqrt{2\pi}} \right) \exp \left[-\frac{1}{2} \left(\frac{x}{a_{\text{ho}} \sigma_U} \right)^2 \right]. \quad (9)$$

Here γ is a dimensionless strength parameter, and σ_U is the standard deviation of the potential's shape (in units of a_{ho}).

For $\bar{N} = 10$, $\gamma = 0.4$, and $\sigma_U = 1$, one obtains the results shown in Figure 4. The simulation was carried out on a $M = 60$ lattice with $L = 12a_{\text{ho}}$, and $S = 10^4$ trajectories. We calculate the correlations between particles in the middle of the cloud and in the wings. Such ranged two-body correlations give insight into what behaviour may be expected to be typical during a single experimental run. The first-order correlation function

$$g^{(1)}(0, x) = \frac{\langle \hat{\Psi}^\dagger(0) \hat{\Psi}(x) \rangle}{\sqrt{\rho(0) \rho(x)}}, \quad (10)$$

describes coherence between particles, where the density is $\rho(x) = \langle \hat{\Psi}^\dagger(x) \hat{\Psi}(x) \rangle$. The second-order (number) correlation function

$$g^{(2)}(0, x) = \frac{\langle \hat{\Psi}^\dagger(0) \hat{\Psi}^\dagger(x) \hat{\Psi}(0) \hat{\Psi}(x) \rangle}{\rho(0) \rho(x)} \quad (11)$$

describes number correlations. That is, when $g^{(2)}(0, x) > 1$, the likelihood of observing a pair of particles with one in the centre of the trap (“0”), and one at

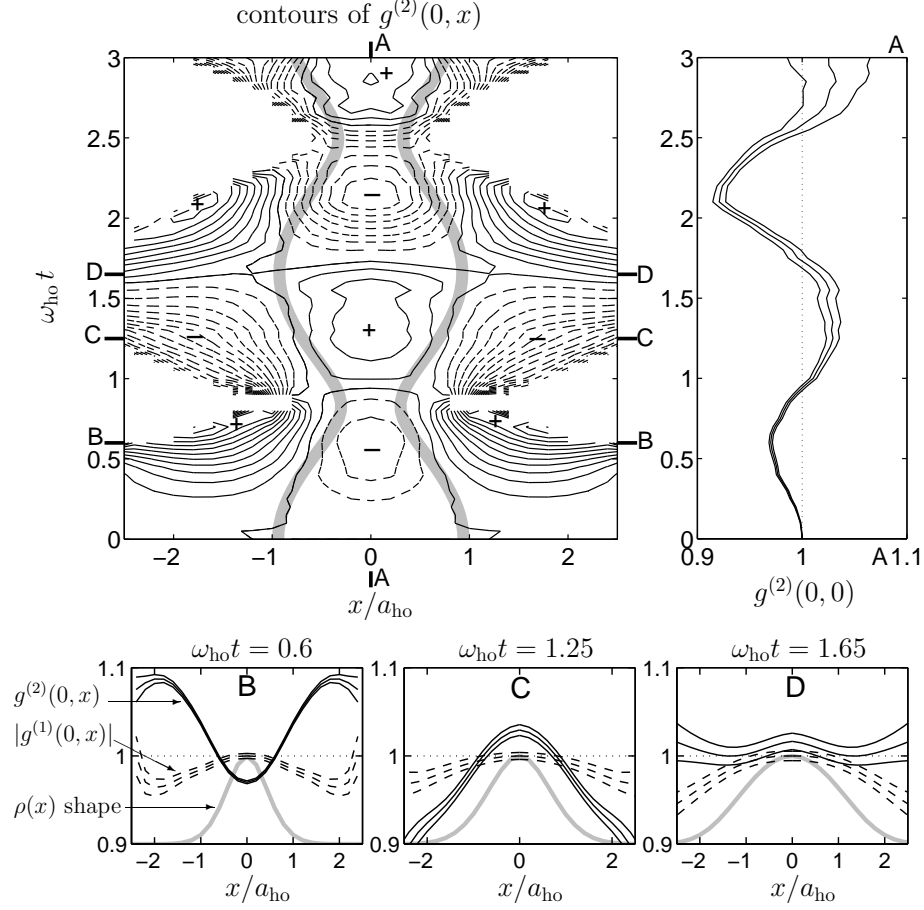


Figure 4: Dynamics of correlations with long-range interactions.

x is increased with respect to the baseline case where the occupation at these points is uncorrelated and given purely by the local densities. In the largest panel, contours of the number correlation function $g^{(2)}$ are plotted, with solid contours indicating $g^{(2)}(0, x) \geq 1$, dashed contours indicating $g^{(2)}(0, x) < 1$. Contour spacing is 0.01. The thick grey lines indicate the rms width of the cloud density $\rho(x)$. In panels A–D, triple lines indicate one-sigma uncertainty, solid lines show $g^{(2)}$, dashed lines show the coherence $|g^{(1)}|$, and solid thick grey lines the density $\rho(x)$.

Notable features seen include the following.

- In the middle of the trap, there is an oscillation between bunching ($g^{(2)}(0, 0) > 1$) and antibunching ($g^{(2)}(0, 0) < 1$).
- This oscillation is *out of phase* (by approximately $\pi/2$) with respect to the

breathing motion of the gas cloud, and the behaviour of pair correlations is quite counter-intuitive. In particular,

- When the particle cloud is contracting, *antibunching* appears at the center of the trap despite a net motion of particles into this region, while simultaneously there is an enhanced likelihood of pairs of atoms with one in the outer region of the cloud and one in the center.
- During expansion, on the other hand, the particles in the center of the trap tend to appear there in pairs despite the net flow of particles out of this region, while pairs of particles with one in the tails, one in the center are suppressed.
- The oscillations of $g^{(2)}(0,0)$ (at the center of the trap) become more pronounced with time. This may indicate a resonance between the breathing and the repulsion, although it is also possible that this is a transient initial effect.
- Coherence between the center of the trap and outlying regions of the cloud deteriorates as time proceeds.

5 General phase-space representations

Finally, we show how these coherence-theory methods can be generalised to incorporate other kinds of correlation into the basis. Most generally, the phase-space approach can be defined as an expansion of the density matrix $\hat{\rho}$, using nonorthogonal operators $\hat{\Lambda}(\vec{\lambda})$, such that:

$$\hat{\rho} = \int P(\vec{\lambda}) \hat{\Lambda}(\vec{\lambda}) d\vec{\lambda} \quad (12)$$

Provided suitable differential identities exist, and that it is possible to integrate by parts, quantum dynamics is transformed to a set of stochastic trajectories in the generalized phase-space variable $\vec{\lambda}$. A different basis choice leads to a different representation. Thus, for example, in the positive P-representation, $\hat{\Lambda}(\vec{\lambda})$ is the off-diagonal coherent-state projector appearing in equation Eq. (3). There are a number of clear trade-offs, in that a variance can be transferred from the distribution to the basis, in order to obtain reducing trajectory spread, leading to lower sampling error. This is shown schematically in Fig (5).

5.1 General M -mode Gaussian operator

Many possible basis sets can be used. As a generic form applicable to both fermionic and bosonic cases, we may consider a Gaussian operator basis, defined here as the normally ordered exponential of a quadratic form in the $2M$ -vector mode operator $\delta\hat{\underline{a}} = (\hat{\mathbf{a}}, \hat{\mathbf{a}}^\dagger) - \underline{a}$, where \underline{a} is a c-vector and $\hat{\mathbf{a}}$ is the vector of annihilation operators. The bosonic kernel[26], with a similar result for fermions[27],

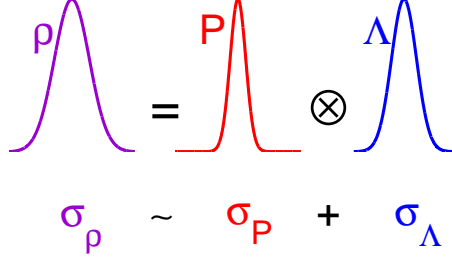


Figure 5: Schematic diagram of how density matrix operator variances are composed of a distribution variance and a basis variance.

is:

$$\hat{\Lambda}(\vec{\lambda}) = \frac{\Omega}{\sqrt{|\underline{\sigma}|}} : \exp \left[-\delta \hat{\underline{a}}^\dagger \underline{\sigma}^{-1} \delta \hat{\underline{a}} / 2 \right] : . \quad (13)$$

Here the ‘quantum phase space’ is extended even further, to the vector: $\vec{\lambda} = (\Omega, \underline{\alpha}, \underline{\sigma})$. This now includes the covariance $\underline{\sigma}$, which can be readily parametrized in terms of normal and anomalous Green’s functions, denoted \mathbf{n} and \mathbf{m} respectively:

$$\underline{\sigma} = \begin{bmatrix} \mathbf{I} + \mathbf{n} & \mathbf{m} \\ \mathbf{m}^+ & \mathbf{I} + \mathbf{n}^T \end{bmatrix} . \quad (14)$$

When $\mathbf{n} = \mathbf{m} = \mathbf{0}$, the representation reduces to that of the positive-P. However with these new parameters, the representation is complete (for number-conserving systems) when the coherent amplitudes are zero, thus allowing for representation of Fermions.

In summary, the Gaussian representation phase space is $\vec{\lambda} = (\Omega, \underline{\alpha}, \underline{\beta}, \mathbf{n}, \mathbf{m}, \mathbf{m}^+)$, where Ω is a weight factor, α, β are (for bosons) coherent amplitudes, \mathbf{n} is number correlations and \mathbf{m}, \mathbf{m}^+ are squeezing correlations.

5.2 Weighted stochastic gauge equations

The use of phase-space methods has a fundamental philosophy of attempting to transform **hard** quantum problems into **tractable** stochastic equations. However, there are several ways to do this, due to the overcompleteness of the basis set. For a basis set that is analytic in the phase-space variables, one can show that, provided partial integration is possible, one can obtain an equivalence class of stochastic equations. These include an arbitrary ‘stochastic gauge’ function \mathbf{g} [28], and have the generic structure:

$$\begin{aligned} d\Omega/\partial t &= \Omega [U + \mathbf{g} \cdot \boldsymbol{\zeta}] \\ d\boldsymbol{\alpha}/\partial t &= \mathbf{A} + \mathbf{B}(\boldsymbol{\zeta} - \mathbf{g}) . \end{aligned} \quad (15)$$

In principle, the Gaussian basis allows a wide range of fermionic and bosonic systems to be simulated from first principles[29]. Nevertheless, there are un-

solved problems that remain (see e.g. [30]). The chief issue is the sampling error, since typically many stochastic trajectories are needed to control growing sampling errors, which eventually become too large for useful results. The sampling error can be improved through careful choice of the gauge function \mathbf{g} , which is a function chosen to stabilize trajectories, as well as the basis set itself, and the details of the simulation method.

6 Summary

In summary, we have described areas of recent development — one experimental and one theoretical — in many-body quantum physics that can be traced from the coherence theory that originated in quantum optics.

Experiments in ultracold atoms are increasingly able to probe the quantum correlations that arise from the many-body nature of the system. We have here been able to describe just two — those involving dynamical collisions of dense clouds — but there are many others.

In parallel, coherence theory has lead to a range of powerful phase-space techniques to simulate many-body quantum dynamics. We have discussed the positive-P approach and its generalisation, the generalised Gaussian method. These methods give rise to representations for bosons **and** fermions, and can deal with either local or nonlocal interactions. One can readily perform three-dimensional lattice simulations, with up to up to 10^{23} particles, and 10^6 modes. The fact that sampling errors increase with time is a serious limitation, however.

Novel physical effects found in the simulations include evaporative heating (not cooling) of center of mass temperatures, and an unexpected atomic anti-bunching effect during compression of a condensate with long-range interactions.

There are many interesting challenges and new quantum physics to be investigated with these approaches. As well as ultra-cold atoms, other complex systems may be investigated, ranging from nanotechnology, through to biochemistry and genetics [31].

Acknowledgements

We acknowledge funding from the Australian Research Council Centre of Excellence program, and useful discussions with K.V. Kheruntsyan. This work was also supported financially by the NWO as part of the FOM quantum gases project.

References

- [1] J. M. Vogels, K. Xu, W. Ketterle. *Phys. Rev. Lett.*, 89:020401, 2002.

- [2] T. Jeltès, J. M. McNamara, W. Hogervorst, W. Vassen, V. Krachmalnicoff, M. Schellekens, A. Perrin, H. Chang, D. Boiron, A. Aspect, C. I. Westbrook. *Nature*, 445(7126):402–405, 2007.
- [3] C. I. Westbrook et. al. arXiv:quant-ph/0609019.
- [4] A. Perrin, H. Chang, V. Krachmalnicoff, M. Schellekens, D. Boiron, A. Aspect, C. I. Westbrook. arXiv:0704.3047v1.
- [5] R. G. Dall, A. G. Truscott. *Optics Communications*, 270(2):255–261, 2007.
- [6] U. Schollwöck. *Rev. Mod. Phys.*, 77:259, 2005.
- [7] W. Kohn. *Rev. Mod. Phys.*, 71:1253, 1999.
- [8] R J Glauber. *Phys. Rev.*, 131(6):2766, 1963.
- [9] E C G Sudarshan. *Phys. Rev. Lett.*, 10(7):277, 1963.
- [10] E. P. Wigner. *Phys. Rev.*, 40:749–759, 1932.
- [11] K Husimi. *Proc. Phys. Math. Soc. Jpn*, 22:264, 1940.
- [12] G. S. Agarwal, E. Wolf. *Phys. Rev. D*, 2(10):2161–2186, Nov 1970.
- [13] G. S. Agarwal, E. Wolf. *Phys. Rev. D*, 2(10):2187–2205, Nov 1970.
- [14] M Lax. *Phys. Rev.*, 145(1):110 – &, 1966.
- [15] P. D. Drummond, C. W. Gardiner. *J. Phys. A*, 13:2353–2368, 1980.
- [16] S Chaturvedi, P Drummond, D F Walls. *J. Phys. A*, 10(11):L187–L192, 1977.
- [17] S. J. Carter, P. D. Drummond, M. D. Reid, R. M. Shelby. *Phys. Rev. Lett.*, 58:1841–1844, 1987.
- [18] P. D. Drummond, J. F. Corney. *Phys. Rev. A*, 60:R2661, 1999.
- [19] Uffe V. Poulsen, Klaus Mølmer. *Phys. Rev. A*, 64(1):013616, Jun 2001.
- [20] P. Deuar, P. D. Drummond. *J. Phys. A*, 39:1163, 2006.
- [21] M R Dowling, P D Drummond, M J Davis, P Deuar. *Phys. Rev. Lett.*, 94(13):130401, 2005.
- [22] I. Carusotto, Y. Castin, J. Dalibard. *Phys. Rev. A*, 63:023606, 2001.
- [23] C. M. Savage, P. E. Schwenn, K. V. Kheruntsyan. *Phys. Rev. A*, 74:033620, 2006.
- [24] P. Deuar, 2005. PhD Thesis, The University of Queensland, arXiv/cond-mat/0507023.

- [25] Franco Dalfovo, Stefano Giorgini, Lev P. Pitaevskii, Sandro Stringari. *Rev. Mod. Phys.*, 71(3):463–512, Apr 1999.
- [26] J F Corney, P D Drummond. *Phys. Rev. A*, 68(6):63822, 2003.
- [27] J. F. Corney, P. D. Drummond. *Phys. Rev. B*, 73:125112, 2006.
- [28] P Deuar, P D Drummond. *Phys. Rev. A*, 66(3):33812, 2002.
- [29] J. F. Corney, P. D. Drummond. *Phys. Rev. Lett.*, 93:260401, 2004.
- [30] F. F. Assaad, P. Werner, P. Corboz, E. Gull, M. Troyer. *Phys. Rev. B*, 72:224518, 2005.
- [31] P. D. Drummond. *Eur. Phys. Jour. B.*, 38(4):617 – 634, 2004.